


Communication

Facile Production of a Fenton-Like Photocatalyst by Two-Step Calcination with a Broad pH Adaptability

Siyang Ji, Yanling Yang, Xing Li, Hang Liu and Zhiwei Zhou * 

College of Architecture and Civil engineering, Beijing University of Technology, No.100 Xi Da Wang Road, Chao Yang District, Beijing 100124, China; jsy_3021826@163.com (S.J.); yangyanling@bjut.edu.cn (Y.Y.); lixing@bjut.edu.cn (X.L.); liuhang98596@163.com (H.L.)

* Correspondence: hubeizhouzhiwei@163.com; Tel.: +86-10-6739-1726

Received: 30 December 2019; Accepted: 31 March 2020; Published: 3 April 2020



Abstract: A novel heterogeneous Fenton-like photocatalyst, Fe-doped graphitic carbon nitride (Fe-g-C₃N₄), was produced by facile two-step calcination method. This Fe-g-C₃N₄ catalyzed rhodamine B degradation in the presence of H₂O₂ accompanied with visible light irradiation. transmission electron microscopy(TEM), x-ray diffraction (XRD), FT-IR, x-ray photoelectron spectroscopy (XPS), and photoluminescence fluorescent spectrometer (PL) characterization analysis methods were adopted to evaluate the physicochemical property of samples. It can be observed that the Fe-g-C₃N₄ exhibited excellent photocatalytic Fenton-like activity at a wide pH range of 3–9, with rhodamine B(RhB) degradation efficiency up to 95.5% after irradiation for 45 min in the presence of 1.0 mM H₂O₂. Its high activity was ascribed to the formation of Fe–N ligands in the triazine rings that accelerated electron movement driving the Fe(III)/Fe(II) redox cycle, and inhibited photo-generated electron hole re-combinations for continuous generation of reactive oxygen species by reactions between Fe(II) and H₂O₂. The main active oxygen species were hydroxyl radicals, followed by superoxide radicals and hole electrons. This produced catalyst of Fe-g-C₃N₄ shows excellent reusability and stability, and can be a promising candidate for decontamination of wastewater.

Keywords: Fenton-like photocatalysis; graphitic carbon nitride; two-step calcination; composite materials

1. Introduction

Advanced oxidation process such as the Fenton reaction and photocatalysis has been extensively studied due to their high degradation activity toward the refractory organic pollutants in recent years [1]. The Fenton reaction has been proven to mineralize most of the organic pollutants [2]. However, the conventional homogeneous Fenton process suffers from the narrow pH range and large amounts of iron precipitation sludge [3]. To overcome these shortcomings, researchers worldwide have focused on the heterogeneous Fenton reaction that immobilizes iron species on the carriers such as clays [4], zeolites [5], and photocatalytic compounds. Furthermore, introducing the Fe–N ligands can effectively increase the pH range of the conventional Fenton reaction [6]. Ligands such as phthalocyanines and tetra-amido macrocyclic can form Fe–N ligands. For example, Gupta et al. used the Fe–TAML catalysts to degrade pentachlorophenol at a high pH of 10 [7]. Zhu et al. developed a Fe(II)-phthalocyanine compound for the degradation of antibiotic carbamazepine [8]. The formation of Fe–N ligands not only stabilizes the iron species, but also accelerates the Fe(III)/Fe(II) redox cycle, thus resulting in the ability to work at higher pH values [9].

Graphitic carbon nitride (g-C₃N₄) is a polymer that combines superior photocatalytic properties with chemical stability [10]. It is easy to prepare through the one-step polymerization of cheap precursors of melamine, cyanoguanidine, and urea [11], and it contains structures with six nitrogen lone-pair electrons, which are ideal sites for chemical modification. However, the fast electron-hole recombination

limited the application of one-step g-C₃N₄. Common modification methods are thermal oxidation exfoliation and surface modification with other ions [12]. On one hand, the two-step calcination (thermal oxidation exfoliation) could potentially improve the photocatalytic activity of one-step g-C₃N₄ by increasing specific surface area and electron transport ability [13]. On the other hand, g-C₃N₄ doping with metal atoms such as Co, Fe, Cu, and Pb can enhance photocatalytic and oxygen-reduction activity. Wang et al. [14] used a one-step calcination method to prepare CoS₂/g-C₃N₄-rGO for reduction of Cr (VI). Guo et al. [15] used one-step calcination method to synthesize a novel Fe₂O₃@g-C₃N₄ for the degradation of tetracycline. Dong et al. [16] developed Cu-g-C₃N₄ by a modified impregnation method to degrade rhodamine B (RhB). Under visible light irradiation in the presence of H₂O₂, the Fenton-like photocatalysis of the above multifunctional compounds will take place, accompanying photoelectron-hole pairs that are generated and active radicals are produced that can degrade organic pollutants [17], meanwhile synergistic effects result from a combination with the Fenton reaction [18]. Specifically, photocatalysis can be combined with Fenton-like oxidation technology, on one hand, photo-generated electrons can promote the reduction of Fe³⁺; on the other hand, H₂O₂ in the Fenton reaction reacting with photo-generated electrons can reduce the electrons-hole recombination probability, thereby improving photocatalytic degradation efficiency [19,20].

Herein, we synthesized a Fenton-like photocatalyst by two-step calcination that doped Fe upon g-C₃N₄. The Fe-g-C₃N₄ catalysts were systematically characterized. Synergistic degradation of RhB by Fenton-like photocatalysis was investigated. The high pH adaptation from 3 to 9 was assessed, and the main active species and mechanism of reaction were clarified.

2. Materials and Methods

2.1. Materials

All chemical reagents used in these experiments were at least of analytical grade. Urea (CH₄N₂O, ≥98.5%), iron chloride hexahydrate (FeCl₃·6H₂O, 99.0%), isopropyl alcohol (IPA, ≥99.5%), ethylenediaminetetraacetic acid disodium salt (EDTA-2Na, 99.0%), and RhB were purchased from Aladdin Industrial Corporation (Shanghai, China). All chemicals were used as received without further purification. Stock solutions were prepared with Milli-Q ultrapure water.

2.2. Preparation of the Catalysts

Urea and FeCl₃·7H₂O were used for the preparation of the calcination of g-C₃N₄ and Fe-g-C₃N₄. The two-step calcination of g-C₃N₄ was optimized according to the method described in a previous study with modifications [21]. One-step calcination (product with prefix '1st') was performed by heating 5 g urea with or without 0.105 g FeCl₃·7H₂O to 550 °C at 5 °C/min for 4 h in a muffle furnace. For two-step calcination ('2nd'), the calcinated products were allowed to spontaneously cool to room temperature, followed by a 2 h-calcination step in a tube furnace at 520 °C (5 °C/min) in a nitrogen atmosphere (Figure 1a).

2.3. Characterization

The morphology of the products was characterized by field-emission scanning electron microscopy (FE-SEM, SU-8020, Hitachi, Tokyo, Japan) and high-resolution transmission electron microscopy (FEI, Tecnai G2 F20, USA). Their crystal structure was determined by x-ray diffraction (XRD-7000, Shimadzu, Kyoto, Japan) using CuKα radiation with 2θ set from 10 to 80°. Fourier transform infrared (FTIR) was recorded with a NICOLET iS10 FTIR spectrometer. Surface chemical composition was analyzed by x-ray photoelectron spectroscopy (XPS, Thermo Fisher Scientific, Waltham, USA) with a monochromatic Al Kα source (1486.6 eV). All binding energies were calibrated based on the C1s peak at 284.8 eV. The specific surface area was measured by nitrogen adsorption-desorption isotherms at 77 K using the Barret-Joyner-Hallender method (NOVA 3200e Sorptometer, Quantachrome, Florida, USA). The optical properties of the catalysts were analyzed by a photoluminescence fluorescent spectrometer (PL,

FLS980, Livingston, Edinburgh) and an ultraviolet-visible diffuse reflectance spectrometer (UV-Vis DRS; 3600 plus, Shimadzu, Kyoto, Japan), respectively. Presence of free radicals was confirmed by electron paramagnetic resonance (EPR) (JES-FA200 JEOL, Tokyo, Japan) under visible light irradiation using 5,5-Dimethyl-1-pyrroline N-oxide (DMPO) as a trapping compound.

2.4. Degradation Performance of the Catalysts

The catalytic activity of the obtained catalysts were evaluated by RhB degradation efficiency at room temperature. For photocatalysis or Fenton-like photocatalysis, a 300W Xe lamp (CEAULIGHT, CEL-HXF300E7, Beijing, China) equipped with a 400 nm UV filter was used that emitted visible light (400–780 nm) at 280 mW/cm². RhB was used as the target pollutant at an initial concentration of 10 mg/L (filtered through 0.45-µm acetate membranes prior to use).

For the photocatalysis reaction, as a typical process, 0.02 g of the catalyst (g-C₃H₄ and Fe-g-C₃H₄) was added into 100 mL RhB solution (10 mg/L). Before irradiation, the suspension was stirred for 40 min in the dark to ensure light-independent adsorption-desorption equilibriums had been reached (presented in Supplementary Materials in Figure S1). Then, a 300 W Xe lamp equipped with a cut off filter (>420 nm) as a light source and placed 12 cm above the surface of the reaction solution was turned on.

For the Fenton-like photocatalysis reaction, under the same condition as the photocatalysis reaction, except that 1.0 mmol/L H₂O₂ was added into the suspension before the irradiation, the doses of which were determined by our pre-experiments (Figure S2). A sample without any catalyst control was included as the control. At a specific time interval, 3 mL of the suspension solution was collected and filtered through a 0.22 µm filter for measure by a UV-Vis Spectrophotometer (UV-2600, SOPTOP, China) at 554 nm. When studying the influence of pH, 0.1 mol/L HCl and NaOH solutions were employed to adjust the initial pH value. The influence of pH on the treated solution during the reaction was not addressed, since the fluctuations of pH value were small (±0.2) [22].

The degradation kinetics of RhB in photocatalysis or the Fenton-like photocatalysis process were fitted based on a pseudo-first-order kinetic model (Equation (1)), where C₀ (mg/L) is the concentration of RhB after adsorption in dark (mg/L), C_t is the concentration at time t (min), and k (min⁻¹) is the pseudo first-order rate constant.

$$\ln C_t/C_0 = -kt \quad (1)$$

The stability and reusability of the synthesized catalysts were tested by repeating the Fenton-like photocatalysis experiment. For this, at the end of a photocatalytic experiment, the used Fe-g-C₃N₄ was filtrated, washed, and dried before being used for the following test.

3. Results

3.1. Characterization

TEM images of the two calcination products were similar, but the material turned from flaxen-collared to brownish upon Fe doping (Figure 1b,c). Element mapping of Fe-g-C₃N₄ (Figure 1d-g) confirmed the presence of Fe responsible for the color change. The Fe-signal overlapped with that of N, indicating interactions between Fe and N. One-step or two-step calcination of Fe-g-C₃N₄ resulted in a nanosheet structure similar to that of g-C₃N₄ visible by SEM (Figure S2). The S_{BET} of 1st g-C₃N₄, 2nd g-C₃N₄, 1st Fe-g-C₃N₄ and 2nd Fe-g-C₃N₄ was 56.78, 78.54, 45.61, and 63.52 m²/g, respectively, which implies that the two-step calcination can increase pore diameter and the BET specific surface area of both materials (Table S1). The higher surface area and larger pore diameter offer more active sites at the catalyst surface, which potentially enhance catalytic activity.

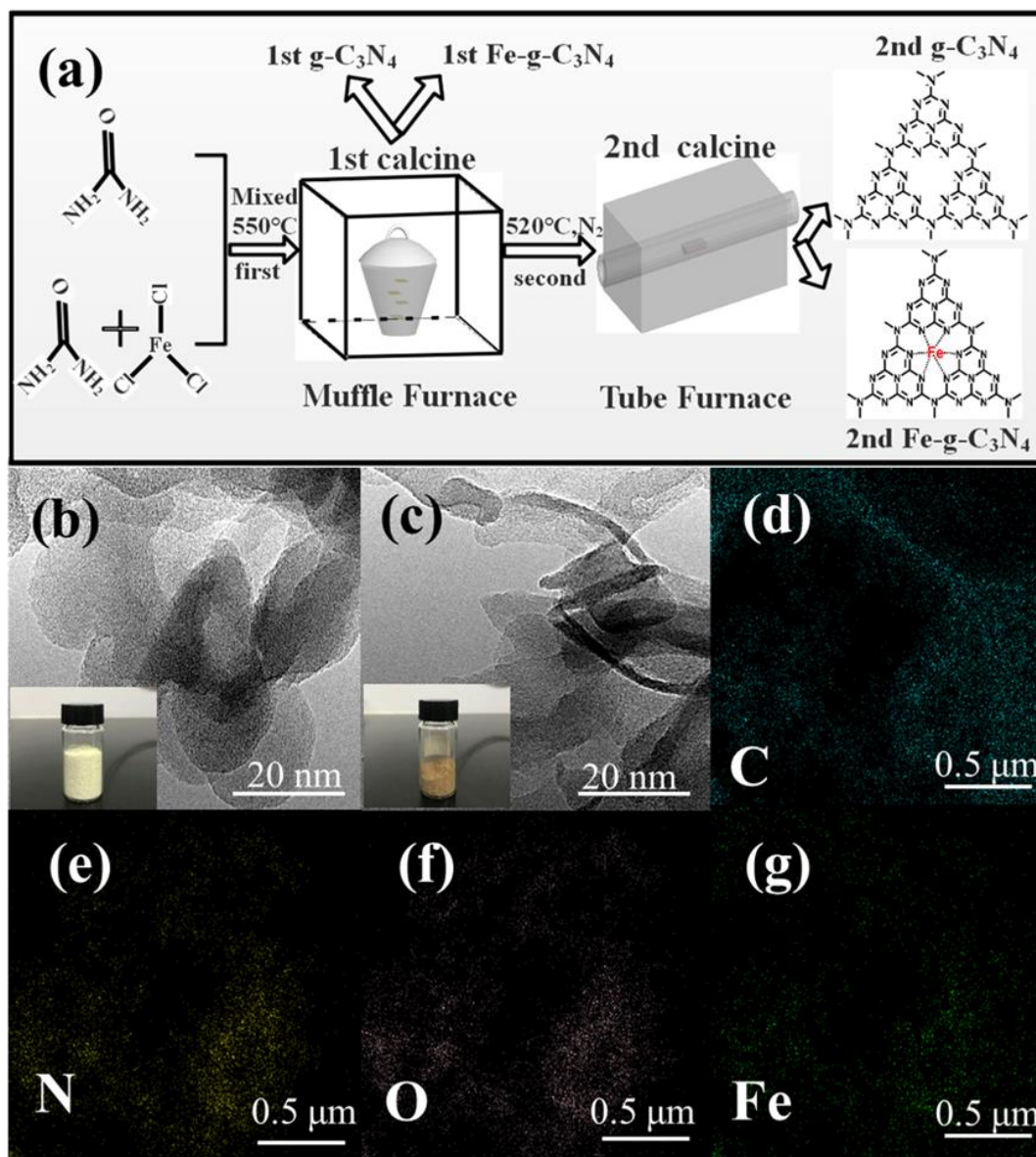


Figure 1. (a) Schematic of the one-step and two-step calcination process for the synthesis of g-C₃N₄ and Fe-g-C₃N₄; (b) TEM images of 2^{nd} g-C₃N₄, and (c) 2^{nd} Fe-g-C₃N₄; (d–g) element mapping of 2^{nd} Fe-g-C₃N₄.

XRD patterns of materials by one-step and two-step calcination (Figure 2a) displayed a peak of the (002) plane around 27.5° , characteristic of a graphite-like structure (JCPDS No. 87-1526). The peak at 13.0° was attributed to the crystal plane of (100) in-planar ordering of tri-s-triazine units [23], and this peak disappeared following Fe-doping, while the peak intensity for the (002) plane was significantly reduced, suggesting the absence of a rigid layer. There were no extra diffraction peaks observed for other phases such as Fe-related secondary phase or impurity, indicating Fe successfully doped into the g-C₃N₄ lattice. The FTIR spectra (Figure 2b) displayed characteristic bands in all samples for stretching vibration of -NH and -NH₂ groups ($3000\text{--}3400\text{ cm}^{-1}$), C=N, and C-N bonds ($1240\text{--}1640\text{ cm}^{-1}$) [24], and triazine (805 cm^{-1}). Iron peaks were not detected in Fe-g-C₃N₄, suggesting that all Fe was doped into the g-C₃N₄.

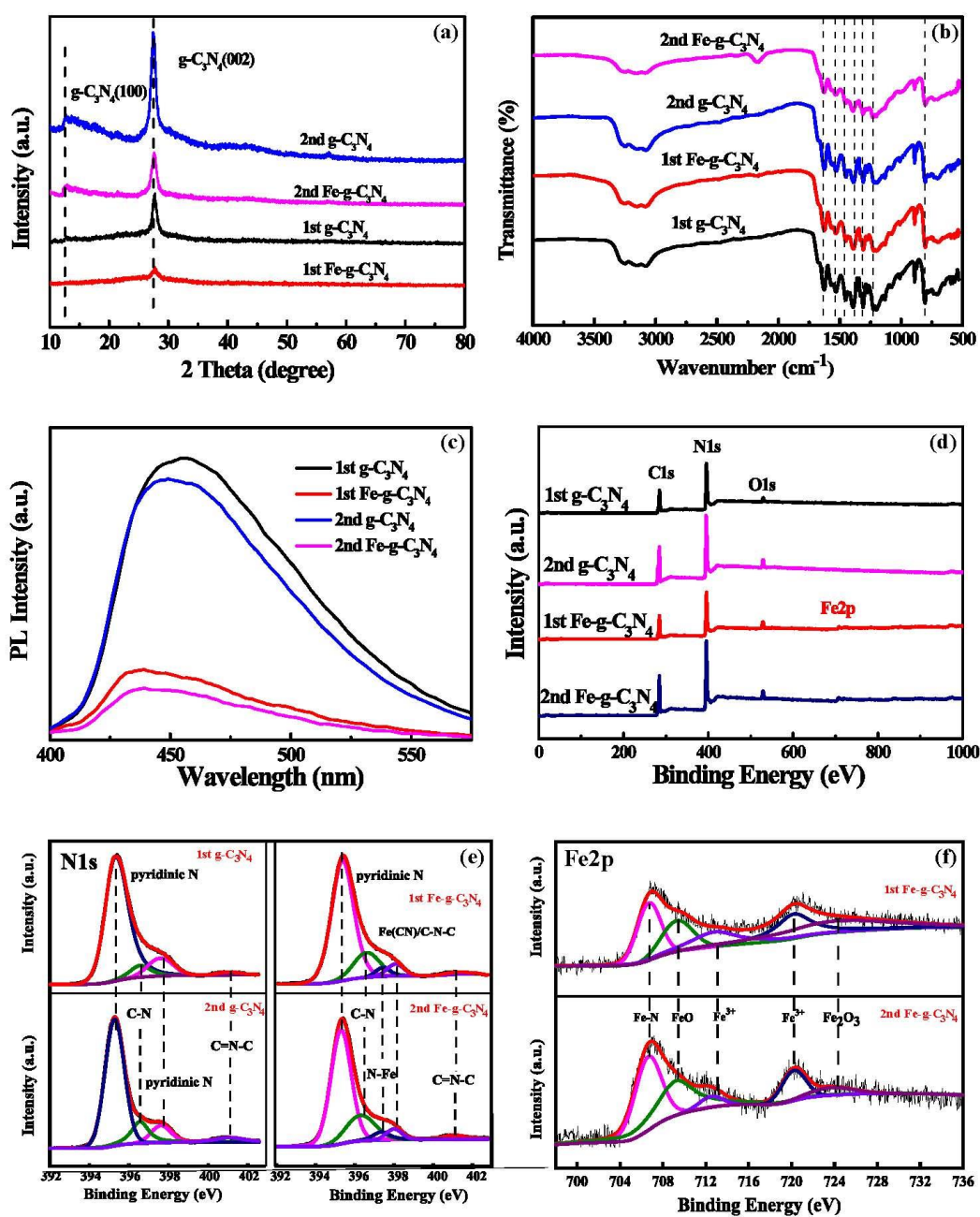


Figure 2. Characterization of one- and two-step $g\text{-C}_3\text{N}_4$ and $\text{Fe-g-C}_3\text{N}_4$ by XRD (a); FTIR (b), photoluminescence (c); and XPS (d–f) with zooms of the N1s (e) and Fe2p (f) spectra.

As shown in Figure 2c, the PL emission of all the samples exhibited a primary emission peak around 450 nm, which is consistent with the earlier reports [25–27]. We found that two-step calcination could reduce peak intensity. As Fe doping strongly reduced peak intensity, probably due to the transfer of photoelectrons to Fe through chemical bridging, resulting in inhibited recombination between photoelectrons and holes [28], this was of benefit to the photocatalytic activity of the catalyst. PL emission spectra are attributed to the band-gap emission in light of its absorption band edge, estimated by the UV–Vis DRS (Figure S4).

The surface chemical state was analyzed by XPS (Figure 2d), and the atomic content was calculated (Table S2). The proportion of Fe element was increased by two-step calcination compared to the one-step products. Peaks in the high-resolution of the N1s and Fe2p spectra were attributed to molecular components. The N1s spectrum of $g\text{-C}_3\text{N}_4$ in Figure 2e contains four peaks that were attributed

to pyridinic N (395.3 and 397.6 eV) [29], C–N (396.6 eV), and C=N–C (401.1 eV), respectively [30]. Fe-doping added peaks at 397.35 and 398.0 eV corresponding to iron nitride (N–Fe) and (Fe–(CN)), respectively [31], accounting for 4.8 and 4.5% of the total N. The Fe2p spectrum in Figure 2g illustrates that surface Fe represents Fe bonded with nitrogen (Fe–N) at 706.7 eV, FeO at 709.3 eV, and Fe₂O₃ at 724.0 eV, comprising 37.8%, 36.9%, and 6.4%, respectively [32,33]. No metallic Fe was detected on the surface of Fe–g–C₃N₄, confirming that all Fe was completely doped into the g–C₃N₄ lattice and mainly in the form of Fe–N.

3.2. Degradation Performance of the Catalysts

The photocatalysis performance of the catalysts were tested under visible light irradiation. As exhibited in Figure 3a, the degradation efficiency of RhB by photolysis can be ignored in the absence of the catalyst, whereas the photocatalytic degradation efficiency of RhB by 2nd g–C₃N₄ was 51.7% within 45 min, which was 13.2% higher than that of 1st g–C₃N₄. The photocatalytic activities were poor for both samples doped with Fe (1st Fe–g–C₃N₄ and 2nd Fe–g–C₃N₄). The sequence of degradation effects from high to low was 2nd g–C₃N₄, 1st g–C₃N₄, 2nd Fe–g–C₃N₄, and 1st Fe–g–C₃N₄. From the fitted curve in Figure 3b, we found the degradation process of RhB conformed to the first-order kinetics model, and the calculated rate constant was 0.01446, 0.01077, 0.00436, 0.00776 min^{−1}, for 2nd g–C₃N₄, 1st g–C₃N₄, 2nd Fe–g–C₃N₄, and 1st Fe–g–C₃N₄, respectively. The photocatalysis performance of 2nd g–C₃N₄ was the best, which was ascribed to the highest S_{BET} (78.535 m²/g) and pore volume (0.383 cc/g) that had the most active sites. It can be concluded that two-step calcination improved properties in the degradation of dyes.

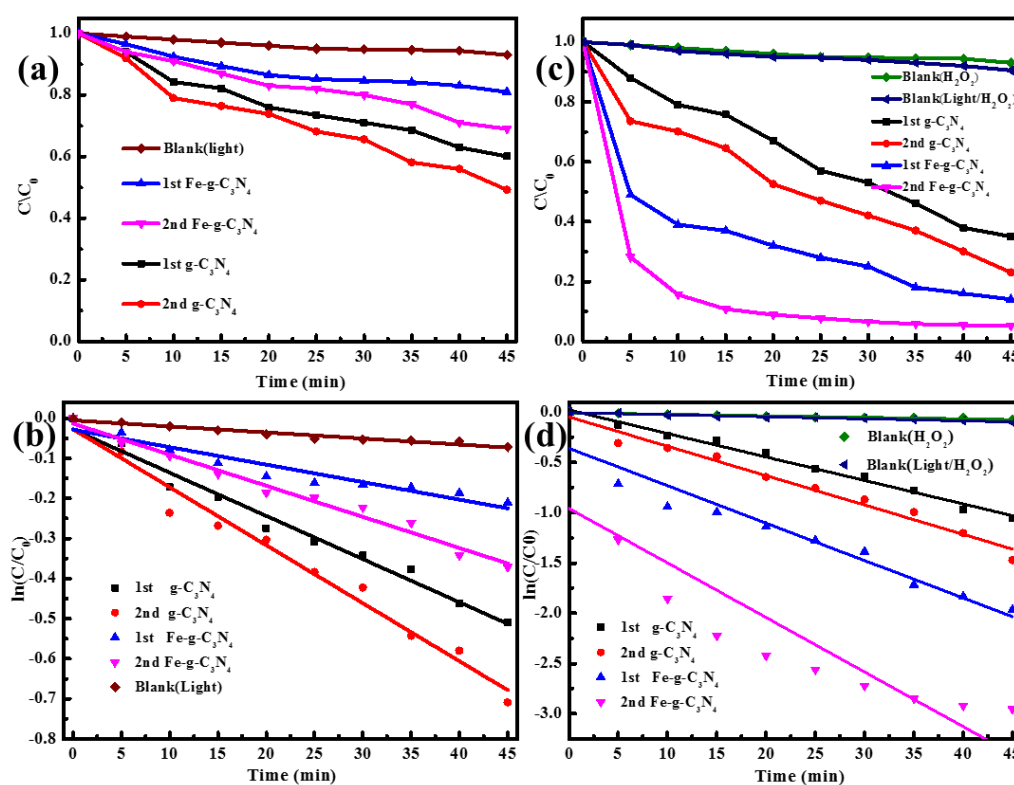


Figure 3. The photocatalysis performance and the pseudo-first-order kinetics fitted curves of RhB (a,b); and Fenton-like photocatalysis performance and the pseudo-first-order kinetics fitted curves of RhB (c,d).

It can be seen from Figure 3c that the degradation efficiency of RhB with the addition of H₂O₂ only reached about 10% at 45 min. The H₂O₂ under visible light without a photocatalyst could not improve

RhB degradation efficiency, both confirming that H_2O_2 only or H_2O_2 with visible light irradiation could marginally degrade RhB [34]. The Fenton-like photocatalysis performance under visible light irradiation in the presence of 1.0 mM H_2O_2 was investigated. In the presence of H_2O_2 , the degradation efficiency of RhB greatly increased after doped Fe ions (Figure 3c). The 2nd Fe-g- C_3N_4 had the highest degradation efficiency, reaching up to 95.5% within 45 min (89% within 15 min). In comparison, the degradation efficiency of RhB by 2nd Fe-g- C_3N_4 under photocatalysis, Fenton-like, and Fenton-like photocatalysis within 45 min was 24.2%, 76.4%, and 95.5%, respectively.

In addition, it can be seen that the 2nd Fe-g- C_3N_4 and 1st Fe-g- C_3N_4 showed higher catalytic activity than that of the 2nd g- C_3N_4 and 1st g- C_3N_4 . The rate constant of the 2nd Fe-g- C_3N_4 (0.5424 min^{-1}) was the highest among all the materials, which was about 1.46, 1.86, and 2.32 times higher than that of the 1st Fe-g- C_3N_4 (0.3722 min^{-1}), 2nd g- C_3N_4 (0.2921 min^{-1}), and 1st g- C_3N_4 (0.2335 min^{-1}). This phenomenon was likely because iron doping can promote the production of active oxygen species [35].

The effect of pH value was tested with the 2nd Fe-g- C_3N_4 only, in the presence of H_2O_2 (Figure 4). It shows that at the pH values of 3, 5, 7, and 9, the degradation efficiency of RhB was 96.0%, 95.2%, 92.9%, and 96.6%. Although RhB degradation was more rapid at a pH of 3, degradation was still highly efficient at a pH of 5–9. The reason is that Fe doping into the g- C_3N_4 formed Fe–N bonds, which promoted the migration and circulation of Fe ions and avoided the precipitation of iron salts during the Fenton-like reaction. This represents a major improvement compared to the classic Fenton reaction, which requires a pH of 2–4. The Fe–N ligand not only keeps the iron stable under different pH values, but also improves the redox properties [36].

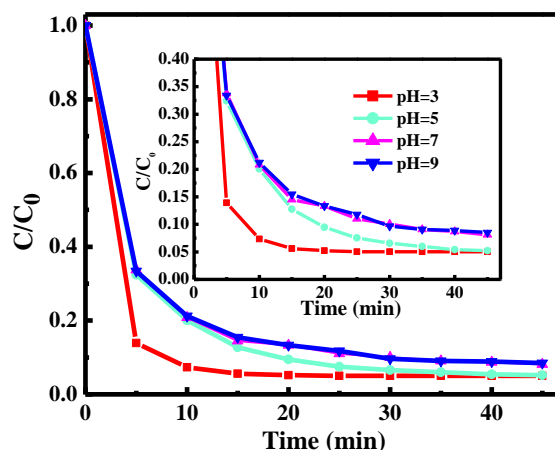


Figure 4. The different pH value of RhB degradation (2nd Fe-g- C_3N_4 only). The solution pH was adjusted by 0.1 mol/L HCl or NaOH, and the pH change of the treated solution was small during the reactions (± 0.2).

We performed recycling tests by recovering the nanoparticles. As shown in Figure 5a, the remove efficiency of RhB by 2nd Fe-g- C_3N_4 had no significant reduction after five cycles, with the degradation efficiency of 95.5%, 94.9%, 93.6%, 92.5%, and 90.3%, respectively. Furthermore, the fresh sample and that used after five times had similar XRD characteristic peaks (Figure 5b). The above results indicate the catalytic had an excellent Fenton-like photocatalytic reusability and stability.

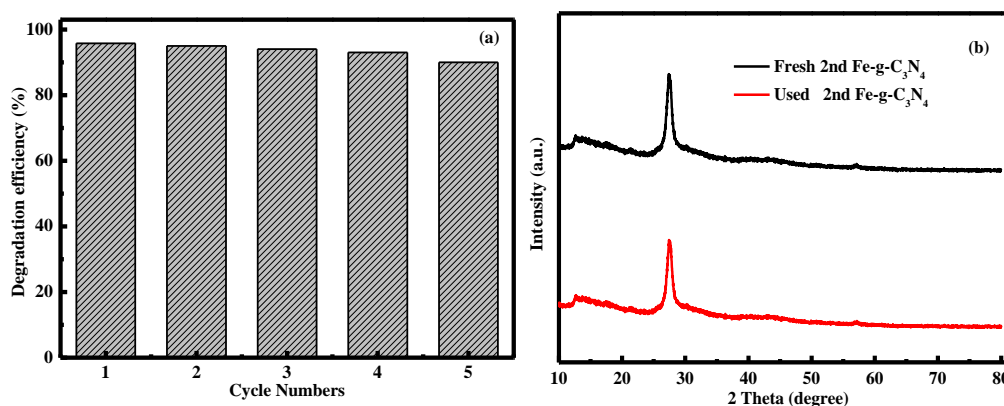


Figure 5. Reusability of the 2nd Fe-g-C₃N₄ after five cycles (a); XRD patterns of the fresh and used 2nd Fe-g-C₃N₄ (b).

3.3. Mechanism of Fenton-Like Photocatalytic Reaction

The reactive species were detected under light and dark conditions by EPR, as shown in Figure 6a,b. Under visible light irradiation, the specific spectrum clearly appeared, which proved the production of $\bullet\text{OH}$ and $\bullet\text{O}_2^-$ during the catalytic process. In order to further prove the main reactive species, trapping tests were carried out. IPA (1 mmol/L) was used as a scavenger of $\bullet\text{OH}$ in the reaction, EDTA-2Na (1 mmol/L) and N₂ were used as scavengers of holes and $\bullet\text{O}_2$ [37], respectively. Compared with the residual RhB (~4%) for 45 min without any scavenger, the residual RhB was 36.7, 8.1, and 17.2% with IPA, EDTA-2Na, and N₂, respectively (Figure 6c). This result indicates that $\bullet\text{OH}$ was the primary reactive species, followed by $\bullet\text{O}_2^-$ and hole electrons.

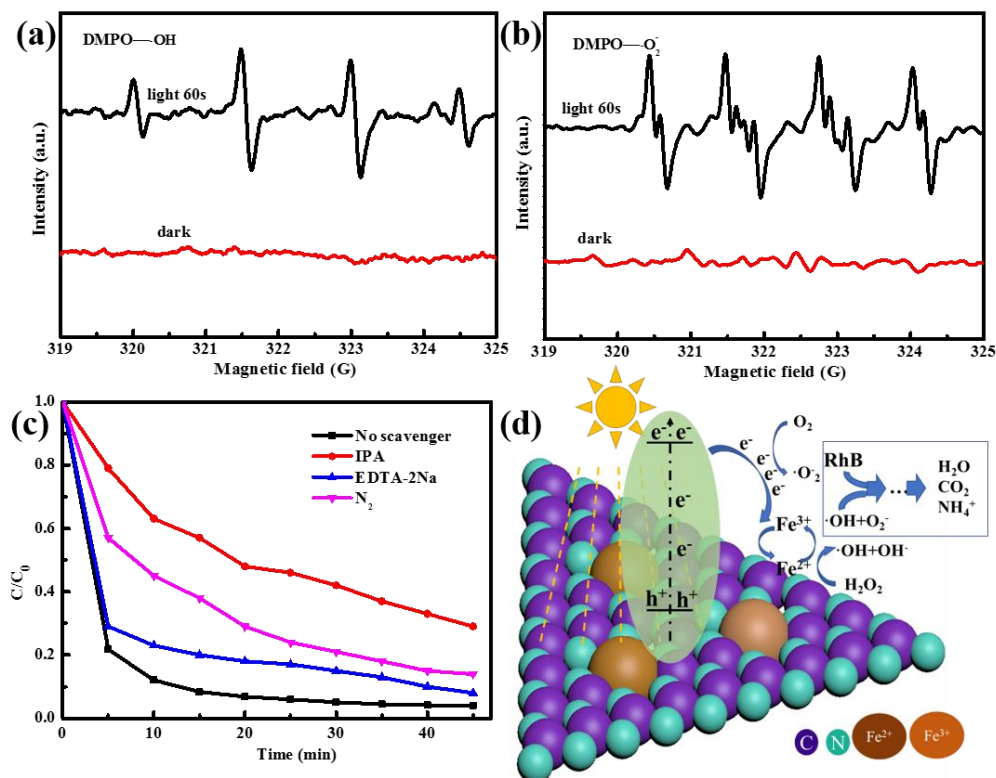


Figure 6. RhB degradation curves with different scavengers over 2nd Fe-g-C₃N₄ (a), EPR spectra of DMPO/ $\bullet\text{OH}$ (b), EPR spectra of DMPO/ $\bullet\text{O}_2^-$ (c), and a schematic illustration of mechanism (d).

Based on the above results and discussion, a tentative mechanism for Fe-g-C₃N₄ dependent Fenton-like photocatalysis is shown in Figure 6d. Fe doped g-C₃N₄, not only led to a soluble and reactive form of iron (Fe(III) and Fe(II)) at different pH values, but also the advantageously modified the redox properties by ligand-field effects [6]. When the Fe-g-C₃N₄ was excited by visible light, the electrons shifted to the conduction band and the holes left in its valence band (Equation (2)). As the interfacial charge transfer effect, parts of the photo-excited electrons reduced Fe(III) into Fe(II) (Equation (3)) (Fe(III)/Fe(II), 0.77 V, vs. NHE) [38]. Normally, the transformation from Fe(III) to Fe(II) is the decisive step for the whole reaction, much lower than the other steps. Nevertheless, it is facilitated with Fe-N ligands, thus created an excellent catalytic ability of Fe-g-C₃N₄. Then, Fe(II) reacted with H₂O₂ to produce •OH (Equation (4)), which oxidized RhB with a high efficiency. Moreover, the photo excited electron could also combine with the dissolved O₂ in the solution to form •O₂⁻ (Equation (5)).



4. Conclusions

In summary, the produced Fe-g-C₃N₄ by two-step calcination was successfully synthesized. Secondary calcination can increase specific surface area and enhance Fenton-like photocatalysis efficiency. When iron was doped into the g-C₃N₄ framework, Fe-N bonds were formed, which could effectively reduce the electron-hole recombination rate and broaden the scope of reaction pH in the range of 3–9. The main active oxygen species were •OH, followed by •O₂⁻ and hole electrons. This produced catalyst of Fe-g-C₃N₄ shows excellent reusability and stability, and can be a promising candidate for dye degradation.

Supplementary Materials: The following are available online at <http://www.mdpi.com/2079-4991/10/4/676/s1>, Figure S1: The dark adsorption of RhB by catalysts, Figure S2: The effects of 2nd Fe-g-C₃N₄ and H₂O₂ concentration on RhB degradation efficiency, Figure S3: SEM micrograph of 1st-g-C₃N₄ (a), 1st Fe-g-C₃N₄ (b), 2nd g-C₃N₄ (c), and 2nd Fe-g-C₃N₄, Figure S4: The UV-Vis diffuse reflectance spectra of 1st g-C₃N₄, 1st-Fe-g-C₃N₄, 2nd g-C₃N₄, and 2nd Fe-g-C₃N₄, Table S1: Structure parameters of the four samples, Table S2: Atomic content (at %) from XPS analysis for samples.

Author Contributions: S.J. and H.L. were responsible for the experimental work, Y.Y. and X.L. supervised the laboratory work, Z.Z. led the research. All authors have read and agreed to the published version of the manuscript.

Funding: This work was realized with the financial support of the National Natural Science Foundation of China (51978006).

Acknowledgments: We give special thanks to Xiaohui Zhang from the CRRC Academy for their kind and valuable discussion and assistance during the paper writing.

Conflicts of Interest: The authors declare no conflicts of interest.

References

1. Zhou, L.; Wang, L.; Zhang, J.; Lei, J.; Liu, Y. Well-Dispersed Fe₂O₃ Nanoparticles on g-C₃N₄ for Efficient and Stable Photo-Fenton Photocatalysis under Visible-Light Irradiation. *Eur. J. Inorg. Chem.* **2016**, *2016*, 5387–5392. [[CrossRef](#)]
2. Klammerth, N.; Malato, S.; Agüera, A.; Fernández-Alba, A.; Mailhot, G. Treatment of Municipal Wastewater Treatment Plant Effluents with Modified Photo-Fenton As a Tertiary Treatment for the Degradation of Micro Pollutants and Disinfection. *Environ. Sci. Technol.* **2012**, *46*, 2885–2892. [[CrossRef](#)] [[PubMed](#)]
3. Hsueh, C.; Huang, Y.; Wang, C.; Chen, C. Degradation of azo dyes using low iron concentration of Fenton and Fenton-like system. *Chemosphere* **2005**, *58*, 1409–1414. [[CrossRef](#)] [[PubMed](#)]

4. Wan, D.; Li, W.; Wang, G.; Chen, K.; Lu, L.; Hu, Q. Adsorption and heterogeneous degradation of rhodamine B on the surface of magnetic bentonite material. *Appl. Surf. Sci.* **2015**, *349*, 988–996. [[CrossRef](#)]
5. Kuźniarska-Biernacka, I.; Raposo, M.M.M.; Baptista, R.M.F.; Parpot, P.; Biernacki, K.; De Magalhães, A.L.; Fonseca, A.; Neves, I. Highly efficient heterogeneous catalysts for phenol oxidation: Binuclear pyrrolyl-azine metal complexes encapsulated in NaY zeolite. *Microporous Mesoporous Mater.* **2016**, *227*, 272–280. [[CrossRef](#)]
6. Georgi, A.; Schierz, A.; Trommler, U.; Horwitz, C.; Collins, T.; Kopinke, F.-D. Humic acid modified Fenton reagent for enhancement of the working pH range. *Appl. Catal. B Environ.* **2007**, *72*, 26–36. [[CrossRef](#)]
7. Gupta, S.S.; Stadler, M.; Noser, C.A.; Ghosh, A.; Steinhoff, B.; Lenoir, D.; Horwitz, C.; Schramm, K.-W.; Collins, T.J. Rapid Total Destruction of Chlorophenols by Activated Hydrogen Peroxide. *Science* **2002**, *296*, 326–328. [[CrossRef](#)]
8. Zhu, Z.; Chen, Y.; Gu, Y.; Wu, F.; Lu, W.; Xu, T.; Chen, W. Catalytic degradation of recalcitrant pollutants by Fenton-like process using polyacrylonitrile-supported iron (II) phthalocyanine nanofibers: Intermediates and pathway. *Water Res.* **2016**, *93*, 296–305. [[CrossRef](#)]
9. Ensing, B.; Buda, F.; Baerends, E.J. Fenton-like chemistry in water: Oxidation catalysis by Fe(III) and H₂O₂. *J. Phys. Chem. A* **2003**, *107*, 5722–5731. [[CrossRef](#)]
10. Li, H.; Deng, P.; Hou, Y. Cobalt disulfide/graphitic carbon nitride as an efficient photocatalyst for hydrogen evolution reaction under visible light irradiation. *Mater. Lett.* **2018**, *229*, 217–220. [[CrossRef](#)]
11. Zheng, Y.; Liu, J.; Liang, J.; Jaroniec, M.; Qiao, S.-Z. Graphitic carbon nitride materials: Controllable synthesis and applications in fuel cells and photocatalysis. *Energy Environ. Sci.* **2012**, *5*, 6717–6731. [[CrossRef](#)]
12. Wang, M.; Yang, W.-H.; Wang, H.-H.; Chen, C.; Zhou, Z.-Y.; Sun, S.-G. Pyrolyzed Fe–N–C Composite as an Efficient Non-precious Metal Catalyst for Oxygen Reduction Reaction in Acidic Medium. *ACS Catal.* **2014**, *4*, 3928–3936. [[CrossRef](#)]
13. Niu, P.; Zhang, L.; Liu, G.; Cheng, H.-M. Graphene-Like Carbon Nitride Nanosheets for Improved Photocatalytic Activities. *Adv. Funct. Mater.* **2012**, *22*, 4763–4770. [[CrossRef](#)]
14. Haghghi, M.; Rahmani, F.; Dehghani, R.; Tehrani, A.M.; Miranzadeh, M.B. Photocatalytic reduction of Cr (VI) in aqueous solution over ZnO/ HZSM-5 nanocomposite: Optimization of ZnO loading and process conditions. *Desalin. Water Treat.* **2017**, *58*, 168–180. [[CrossRef](#)]
15. Guo, T.; Wang, K.; Zhang, G.; Wu, X. A novel α -Fe₂O₃@g-C₃N₄ catalyst: Synthesis derived from Fe-based MOF and its superior photo-Fenton performance. *Appl. Surf. Sci.* **2019**, *469*, 331–339. [[CrossRef](#)]
16. Dong, Q.; Chen, Y.; Wang, L.; Ai, S.; Ding, H. Cu-modified alkalized g-C₃N₄ as photocatalytically assisted heterogeneous Fenton-like catalyst. *Appl. Surf. Sci.* **2017**, *426*, 1133–1140. [[CrossRef](#)]
17. Chatterjee, D.; Dasgupta, S. Visible light induced photocatalytic degradation of organic pollutants. *J. Photochem. Photobiol. C Photochem. Rev.* **2005**, *6*, 186–205. [[CrossRef](#)]
18. Guo, S.; Zhang, G.; Yu, J.C. Enhanced photo-Fenton degradation of rhodamine B using graphene oxide–amorphous FePO₄ as effective and stable heterogeneous catalyst. *J. Colloid Interface Sci.* **2015**, *448*, 460–466. [[CrossRef](#)]
19. Doumic, L.I.; Soares, P.; Ayude, M.A.; Cassanello, M.; Boaventura, R.; Vilar, V.J. Enhancement of a solar photo-Fenton reaction by using ferrioxalate complexes for the treatment of a synthetic cotton-textile dyeing wastewater. *Chem. Eng. J.* **2015**, *277*, 86–96. [[CrossRef](#)]
20. Ortega-Liebana, M.C.; Sánchez-López, E.M.; Hidalgo-Carrillo, J.; Marinas, A.; Marinas, J.; Urbano, F.J. A comparative study of photocatalytic degradation of 3-chloropyridine under UV and solar light by homogeneous (photo-Fenton) and heterogeneous (TiO₂) photocatalysis. *Appl. Catal. B Environ.* **2012**, *127*, 316–322. [[CrossRef](#)]
21. Liu, J.; Liu, Y.; Liu, N.; Han, Y.; Zhang, X.; Huang, H.; Lifshitz, Y.; Lee, S.-T.; Zhong, J.; Kang, Z. Metal-free efficient photocatalyst for stable visible water splitting via a two-electron pathway. *Science* **2015**, *347*, 970–974. [[CrossRef](#)] [[PubMed](#)]
22. Xiong, Z.; Wang, Z.; Muthu, M.; Zhang, Y. Construction of an in-situ Fenton-like system based on a g-C₃N₄ composite photocatalyst. *J. Hazard. Mater.* **2019**, *373*, 565–571. [[CrossRef](#)] [[PubMed](#)]
23. Liu, Q.; Zhang, J. Graphene Supported Co-g-C₃N₄ as a Novel Metal–Macrocyclic Electrocatalyst for the Oxygen Reduction Reaction in Fuel Cells. *Langmuir* **2013**, *29*, 3821–3828. [[CrossRef](#)] [[PubMed](#)]
24. Xu, Y.; Zhang, L.; Yin, M.; Xie, D.; Chen, J.; Yin, J.; Fu, Y.; Zhao, P.; Zhong, H.; Zhao, Y.; et al. Ultrathin g-C₃N₄ films supported on Attapulgite nanofibers with enhanced photocatalytic performance. *Appl. Surf. Sci.* **2018**, *440*, 170–176. [[CrossRef](#)]

25. Xu, J.; Li, Y.; Peng, S.; Lu, G.; Li, S. Eosin Y-sensitized graphitic carbon nitride fabricated by heating urea for visible light photocatalytic hydrogen evolution: The effect of the pyrolysis temperature of urea. *Phys. Chem. Chem. Phys.* **2013**, *15*, 7657. [[CrossRef](#)] [[PubMed](#)]
26. Li, X.; Zhang, J.; Shen, L.; Ma, Y.; Lei, W.; Cui, Q.; Zou, G. Preparation and characterization of graphitic carbon nitride through pyrolysis of melamine. *Appl. Phys. A* **2008**, *94*, 387–392. [[CrossRef](#)]
27. Wang, K.; Li, Q.; Liu, B.; Cheng, B.; Ho, W.; Yu, J. Sulfur-doped g-C₃N₄ with enhanced photocatalytic CO₂-reduction performance. *Appl. Catal. B Environ.* **2015**, *176*, 44–52. [[CrossRef](#)]
28. Hu, J.; Zhang, P.; An, W.; Liu, L.; Liang, Y.; Cui, W. In-situ Fe-doped g-C₃N₄ heterogeneous catalyst via photocatalysis-Fenton reaction with enriched photocatalytic performance for removal of complex wastewater. *Appl. Catal. B Environ.* **2019**, *245*, 130–142. [[CrossRef](#)]
29. Leong, K.H.; Lim, P.F.; Sim, L.C.; Punia, V.; Pichiah, S. Improved solar light stimulated charge separation of g-C₃N₄ through self-altering acidic treatment. *Appl. Surf. Sci.* **2018**, *430*, 355–361. [[CrossRef](#)]
30. Yatsimirskii, K.; Nemoshkalenko, V.; Nazarenko, Y.; Aleshin, V.; Zhilinskaya, V.; Tomashevsky, N. Use of X-ray photoelectron and Mössbauer spectroscopies in the study of iron pentacyanide complexes. *J. Electron Spectrosc. Relat. Phenom.* **1977**, *10*, 239–245. [[CrossRef](#)]
31. Ma, J.Q.; Yang, Q.F.; Wen, Y.Z.; Liu, W.P. Fe-g-C₃N₄/graphitized mesoporous carbon composite as an effective Fenton-like catalyst in a wide pH range. *Appl. Catal. B Environ.* **2017**, *201*, 232–240. [[CrossRef](#)]
32. Maya, L.; Richards, H.L. Polymeric Cyanoborane, (CNBH₂)_n: Single Source for Chemical Vapor Deposition of Boron Nitride Films. *J. Am. Ceram. Soc.* **1991**, *74*, 406–409. [[CrossRef](#)]
33. Li, Z.; Kong, C.; Lu, G. Visible Photocatalytic Water Splitting and Photocatalytic Two-Electron Oxygen Formation over Cu- and Fe-Doped g-C₃N₄. *J. Phys. Chem. C* **2015**, *120*, 56–63. [[CrossRef](#)]
34. Daneshvar, N.; Behnajady, M.A.; Mohammadi, M.K.A.; Dorraji, M.S.S. UV/H₂O₂ treatment of Rhodamine B in aqueous solution: Influence of operational parameters and kinetic modeling. *Desalination* **2008**, *230*, 16–26. [[CrossRef](#)]
35. Chen, J.Y.; Xiao, X.Y.; Wang, Y.; Ye, Z.H. Fabrication of hierarchical sheet-on-sheet WO₃/g-C₃N₄ composites with enhanced photocatalytic activity. *J. Alloys Compd.* **2019**, *777*, 325–334. [[CrossRef](#)]
36. Liu, W.; Ma, J.; Shen, C.; Wen, Y.; Liu, W. A pH-responsive and magnetically separable dynamic system for efficient removal of highly dilute antibiotics in water. *Water Res.* **2016**, *90*, 24–33. [[CrossRef](#)]
37. Alam, U.; Khan, A.; Raza, W.; Khan, A.; Bahnemann, D.W.; Muneer, M. Highly efficient Y and V co-doped ZnO photocatalyst with enhanced dye sensitized visible light photocatalytic activity. *Catal. Today* **2017**, *284*, 169–178. [[CrossRef](#)]
38. Liu, Q.; Guo, Y.R.; Chen, Z.H.; Zhang, Z.Z.; Fang, X.M. Constructing a novel ternary Fe(III)/graphene/g-C₃N₄ composite photocatalyst with enhanced visible-light driven photocatalytic activity via interfacial charge transfer effect. *Appl. Catal. B Environ.* **2016**, *183*, 231–241. [[CrossRef](#)]

